Inorg. Chem. **2002**, *41*, 2574–2582

Hydrolysis of Tin(II) Neo-pentoxide: Syntheses, Characterization, and X-ray Structures of $[Sn(ONep)_2]_\infty$, $Sn_5(\mu_3\text{-}O)_2(\mu\text{-}ONep)_6$, and $Sn_6(\mu_3\text{-}O)_4(\mu\text{-}ONep)_4$ Where ONep = OCH_2CMe_3

Timothy J. Boyle,* Todd M. Alam, Mark A. Rodriguez, and Cecilia A. Zechmann

Sandia National Laboratories, Advanced Materials Laboratory, 1001 University Boulevard, S.E. Albuquerque, New Mexico 87106

Received December 5, 2001

The reaction of $[Sn(NMe_2)_2]_2$ (**1**) with 4 equiv of $HOCH_2CMe_3$ (HONep) leads to the isolation of $[Sn(ONep)_2]_\infty$ (**2**). Each Sn atom is four coordinated with μ-ONep ligands bridging the metal centers; however, if the free electrons of the Sn(II) metal center are considered, each Sn center adopts a distorted trigonal bipyramidal (TBP) geometry. Through ^{119}Sn NMR experiments, the polymeric compound **2** was found to be disrupted into smaller oligomers in solution. Titration of **2** with H_2O led to the identification of two unique hydrolysis products characterized by single-crystal X-ray diffraction as $Sn_5(\mu_3\text{-}O)_2(\mu\text{-}ONep)_6$ (**3**) and $Sn_6(\mu_3\text{-}O)_4(\mu\text{-}ONep)_4$ (**4**). Compound **3** consists of an asymmetrical molecule that has five Sn atoms arranged in a square-based pyramidal geometry linked by four basal μ-ONep ligands, two facial μ_3-O, and two facial μ-ONep ligands. Compound **4** was solved in a novel octahedral arrangement of six Sn cations with an asymmetric arrangement of μ_3-O and μ-ONep ligands that yields two square base pyramidal and four pyramidal coordinated Sn cations. These compounds were further identified by multinuclear (^{1}H, ^{13}C, ^{17}O, and ^{119}Sn) solid-state MAS and high resolution, solution NMR experiments. Because of the complexity of the compounds and the accessibility of the various nuclei, 2D NMR experiments were also undertaken to elucidate the solution behavior of these compounds. On the basis of these studies, it was determined that while the central core of the solid-state structures of **3** and **4** is retained, dynamic ligand exchange leads to more symmetrical molecules in solution. Novel products **3** and **4** lend structural insight into the stepwise hydrolysis of Sn(II) alkoxides.

Introduction

Cassiterite, or tin oxide, thin films are of recent interest for such varied applications as gas sensors (NO_x, CO_x, HOR, CH_4),[1−10] solar cells,[11,12] reversible thermoelectric converters,[13] phosphors,[14] and anodes of Li-ion batteries.[15−17] We favor solution routes to ceramic thin films because of the relatively inexpensive experimental setup, ease of cation variations, and low processing temperatures. This method involves the dissolution of the appropriate precursor(s) in the desired solvent that is then spin-cast deposited onto a substrate followed by thermal treatment. Metal alkoxides

* To whom correspondence should be sent. E-mail: tjboyle@sandia.gov.

(1) Abbas, M. N.; Moustafa, G. A.; Gopel, T. V. *Anal. Chim. Acta* **2001**, *431*, 181.
(2) Chaudhary, B. A.; Mulla, I. S.; Vijayamohanan, K.; Hegde, S. G.; Srinivas, D. *J. Phys. Chem. B* **2001**, *105*, 2565.
(3) Hellegouarc'h, F.; Arefi-Khonsari, F.; Planade, R.; Amouroux, J. *Sens. Actuators, B* **2001**, *73*, 27.
(4) Gregory, O. J.; Luo, Q. *Sens. Actuators, Al* **2001**, *88*, 234.
(5) Tarabek, J.; Wolter, M.; Rapta, P.; Plieth, W.; Maumy, M.; Dunsch, L. *Macromol. Symp.* **2001**, *164*, 219.
(6) Yoshimi, Y.; Ohdira, R.; Iiyama, C.; Sakai, K. *Sens. Actuators, B* **2001**, *73*, 49.
(7) Koh, S. K.; Jung, H. J.; Song, S. K.; Choi, W. K.; Choi, D.; Jeon, J. S. Patent US598990, 1999.
(8) Koh, S. K.; Jung, H. J.; Song, S. K.; Choi, W. K.; Choi, D.; Jeon, J. S. Patent US6059937, 2000.
(9) Chou, J. C.; Chung, W.-Y.; Hsiung, S.-K.; Sun, T.-P.; Liao, H.-K. Patent US6218208, 2001.
(10) Chang, S.-C. Patent US4169369, 1979.
(11) Veluchamy, P.; Tsuji, M.; Nishio, T.; Aramoto, T.; Higuchi, H.; Kumazawa, S.; Shibutani, S.; Nakajima, J.; Arita, T.; Ohyama, H. *Sol. Energy Mater. Sol. Cells* **2001**, *67*, 179.
(12) Amin, N.; Isaka, T.; Yamada, A.; Konagai, M. *Sol. Energy Mater. Sol. Cells* **2001**, *67*, 195.
(13) Yater, J. C.; Yater, J. A.; Yater, J. E. Patent US5889287, 1999.
(14) Chadha, S. S.; Alwan, J. J. Patent US5695809, 1997.
(15) Nam, S. C.; Yoon, Y. S.; Cho, W. I.; Cho, B. W.; Chun, H. S.; Yun, K. S. *Electron. Commun.* **2001**, *3*, 6.
(16) Nam, S. C.; Yoon, Y. S.; Cho, W. I.; Cho, B. W.; Chun, H. S.; Yun, K. S. *J. Electrochem. Soc.* **2001**, *148*, A220.
(17) Mohamedi, M.; Lee, S. J.; Takahashi, D.; Nishizawa, M.; Itoh, T.; Uchida, I. *Electrochim. Acta* **2001**, *46*, 1161.

10.1021/ic011247f CCC: $22.00
Published on Web 04/04/2002

have been found to be excellent solution route precursors because of their high solubility, low decomposition temperatures, ease of modification, hydrolysis cross-linking behavior, and commercial availability.[18−21]

However, to fully exploit the properties of these precursors, it is necessary to know their structures. On the basis of the diverse applications of cassiterite thin films, it is, therefore, surprising that only a few simple tin alkoxide ($Sn(OR)_x$) species have been crystallography characterized, including four Sn(IV) complexes $[Sn(OR)_4(HOR)]_2$ (OR = $OCHMe_2$[22,23] or $OCH_2C(H)Me_2$[24]), $Sn(OCMe_3)_4$,[22] $[Sn(OCH_2Ph)_4(HN(CH_3)_2)]_2$,[25] and two Sn(II) dinuclear complexes, $[Sn(OCMe_3)_2]_2$[26,27] and $[Sn(OC(CH_3)_2-C_6H_4)_2]_2$.[25] A number of Sn(II) and Sn(IV) aryloxide species have been characterized as mono- and dinuclear on the basis of the steric bulk of the ring substituent.[25] Several fluorinated alkoxides have also been identified, including $Sn(OCH(CF_3)_2)_4 \cdot HNMe_2$[28] and $Sn(OCH(CF_3)_2)_2 \cdot HNMe_2$[29] for the production of F-doped tin oxide materials. Independent of the oxidation state of the starting Sn precursor or the ligand set investigated, the final +4 oxidation state is most often observed in the final tin oxide ceramic.[28−35]

We have previously reported on the utility of neopentoxide (ONep = OCH_2CMe_3) derivatives in the preparation of ceramic thin films.[36−44] Therefore, we attempted to synthesize the Sn(II) derivative through the use of an amide−alcohol exchange reaction using $[Sn(NMe_2)_2]_2$ (**1**)[18,45,46] and HONep (eq 1). The product isolated was the novel polymeric Sn(II) alkoxide, $[Sn(\mu\text{-ONep})_2]_\infty$ (**2**).

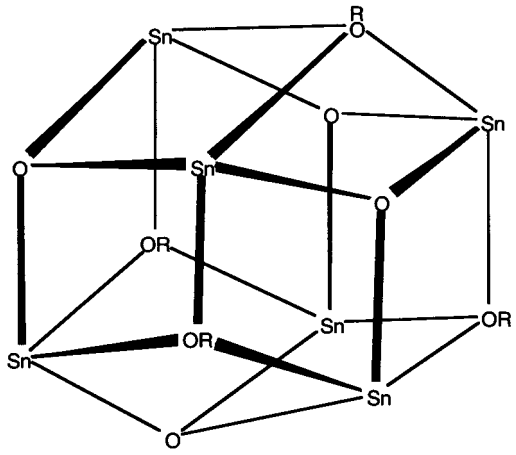

Figure 1. Schematic of central core of $Sn_6(\mu\text{-O})_4(\mu_3\text{-OR})_4$.

$$[Sn(NMe_2)_2]_2 + 4HONep \rightarrow [Sn(ONep)_2]_\infty + 4HNMe_2 \quad (1)$$

The introduction of water (typically through ambient atmospheres) is critical to the formation of the cross-linked M−O−M film network that is necessarily formed during spin-coat deposition processes. However, the rapidity with which metal alkoxides are hydrolyzed by water, the low solubilities of the resultant products, and the complex nature of these species make it difficult to control the properties of the final materials. A full understanding of how metal alkoxides are transformed in the presence of water is necessary to garner greater control over the final ceramic material.

Studies on the hydrolysis of $Sn(OR)_x$ precursors to cassiterite particles have been presented[32,35,47−52] wherein some of these investigations have reported a two-step hydrolysis mechanism.[51,52] The majority of the hydrolyzed $Sn(OR)_x$ species that have been isolated are from the hexanuclear oxo alkoxy family of compounds: $Sn_6(\mu_3\text{-O})_4(\mu_3\text{-OR})_4$ (OR = OH,[48] OMe,[49] $OCHMe_2$,[50] $OSiMe_3$[53]). A schematic of the core of these structures is shown in Figure 1. A $Sn_3(O)(OCH_2C(H)Me_2)_{10} \cdot 2(HOCH_2C(H)Me_2)$ complex was also identified from the partial hydrolysis of the product

(18) Bradley, D. C.; Mehrotra, R. C.; Gaur, D. P. *Metal Alkoxides*; Academic Press: New York, 1978.
(19) Chandler, C. D.; Roger, C.; Hampden-Smith, M. J. *Chem. Rev.* **1993**, *93*, 1205.
(20) Caulton, K. G.; Hubert-Pfalzgraf, L. G. *Chem. Rev.* **1990**, *90*, 969.
(21) Hubert-Pfalzgraf, L. G. *New. J. Chem.* **1987**, *11*, 663.
(22) Hampden-Smith, M. J.; Wark, T. A.; Rheingold, A.; Huffman, J. C. *Can. J. Chem.* **1991**, *69*, 121.
(23) Reuter, H.; Kremser, M. *Z. Anorg. Allg. Chem.* **1991**, *598/599*, 259.
(24) Chandler, C. D.; Caruso, J.; Hampden-Smith, M. J.; Rheingold, A. L. *Polyhedron* **1995**, *14*, 2491.
(25) Smith, G. D.; Visciglio, V. M.; Fanwich, P. E.; Rothwell, I. P. *Organometallics* **1992**, *11*, 1064.
(26) Fjeldberg, T.; Hitchcock, P. B.; Lappert, M. F.; Smith, S. J.; Thorne, A. J. *Chem. Commun.* **1985**, 939.
(27) Veith, M.; Hobein, P.; Rosler, R. *Z. Naturforsch., B: Chem. Sci.* **1989**, *44*, 1067.
(28) Suh, S.; Hoffman, D. M.; Atagi, L. M.; Smith, D. C.; Liu, J.-R.; Chu, W.-K. *Chem. Mater.* **1997**, *9*, 730.
(29) Suh, S.; Hofman, D. M. *Inorg. Chem.* **1996**, *35*, 6164.
(30) Gamard, A.; Jousseaume, B.; Toupance, T.; Campet, G. *Inorg. Chem.* **1999**, *38*, 4671.
(31) Teeramongkonrasmee, A.; Sriyudthsak, M. *Sens.Acutators, B* **2000**, *66*, 256.
(32) Gulliver, E. A.; Garvey, J. W.; Wark, T. A.; Hampden-Smith, M. J.; Datye, A. *J. Am. Ceram. Soc.* **1991**, *74*, 1091.
(33) Park, S. S.; Mackenzie, J. D. *Thin Solid Films* **1995**, *258*, 268.
(34) Park, S. S.; Mackenzie, J. D. *Thin Solid Films* **1996**, *274*, 154.
(35) Hampen-Smith, M. J.; Wark, T. A.; Brinker, C. J. *Coord. Chem. Rev.* **1992**, *112*, 81.
(36) Boyle, T. J.; Alam, T. M.; Mechenbeir, E. R.; Scott, B.; Ziller, J. W. *Inorg. Chem.* **1997**, *36*, 3293.
(37) Boyle, T. J.; Alam, T. M.; Dimos, D.; Moore, G. J.; Buchheit, C. D.; Al-Shareef, H. N.; Mechenbier, E. R.; Bear, B. R. *Chem. Mater.* **1997**, *9*, 3187.
(38) Boyle, T. J.; Bradley, D. C.; Hampden-Smith, M. J.; Patel, A.; Ziller, J. W. *Inorg. Chem.* **1995**, *34*, 5893.
(39) Boyle, T. J.; Schwartz, R. W.; Doedens, R. J.; Ziller, J. W. *Inorg. Chem.* **1995**, *34*, 1110.
(40) Boyle, T. J.; Pedrotty, D. M.; Scott, B.; Ziller, J. W. *Polyhedron* **1997**, *17*, 1959.
(41) Boyle, T. J.; Alam, T. M.; Tafoya, C. J.; Mechenbeir, E. R.; Ziller, J. W. *Inorg. Chem.* **1999**, *38*, 2422.
(42) Boyle, T. J.; Pedrotty, D. M.; Alam, T. M.; Vick, S. C.; Rodriguez, M. A. *Inorg. Chem.* **2000**, *39*, 5133.
(43) Boyle, T. J.; Tyner, R. P.; Alam, T. M.; Scott, B. L.; Ziller, J. W.; Potter, B. G. J. *J. Am. Chem. Soc.* **1999**, *121*, 12104.
(44) Gallegos, J. J. I.; Ward, T. L.; Boyle, T. J.; Francisco, L. P.; Rodriguez, M. A. *Chem. Vap. Deposition* **2000**, *6*, 21.
(45) Harris, D. H.; Lappert, M. F. *Chem. Commun.* **1974**, 895.
(46) Olmstead, M. M.; Power, P. P. *Inorg. Chem.* **1984**, *23*, 413.
(47) Matsumoto, T.; Murakami, Y.; Yahikozawa, K.; Takasu, Y. *Kagaku Kogaku Ronbunshu* **1995**, *21*, 1047.
(48) Howie, R. A.; Moser, W. *Nature* **1968**, *219*, 373.
(49) Harrison, P. G.; Haylett, B. J.; King, T. J. *Chem. Commmun.* **1978**, 112.
(50) Sasaki, Y.; Miyazawa, N. *Kinki Daigaku Rikogakubu Kenkyu Hokoku* **1992**, *28*, 237.
(51) Yang, C. B.; Tung, J. Y.; Chen, J. H.; Liao, F. L.; Wang, S. L.; Wang, S. S.; Hwang, L. P. *J. Chem. Crystallogr.* **1998**, *28*, 481.
(52) Tsai, C. C.; Chen, Y. J.; Chen, J. H.; Hwang, L. P. *Polyhedron* **1992**, *11*, 1647.
(53) Sita, L. R.; Xi, R.; Yap, G. P. A.; Liable-Sands, L. M.; Rheingold, A. L. *J. Am. Chem. Soc.* **1997**, *119*, 756.

from the reaction of $SnCl_4$ and $Na(OCH_2C(H)Me_2)$.[54] The lack of a fully crystallographically characterized, stepwise hydrolysis of a $Sn(OR)_x$ leaves a void in the understanding of how these species are converted to the final ceramic material.

Therefore, we undertook an investigation into the hydrolysis behavior of polymeric **2** through the stoichiometric addition of water (the number of equivalents is noted by value of *n*) to stirring solutions of **2** in THF (eq 2). The products of these reactions were identified by single-crystal X-ray diffraction and heteronuclear (^{17}O and ^{119}Sn) NMR experiments as $Sn_5(\mu_3\text{-}O)_2(\mu\text{-}ONep)_6$ (**3**, $n = {}^2/_5$) and $Sn_6(\mu_3\text{-}O)_4(\mu\text{-}ONep)_4$ (**4**, $n = {}^2/_3$). The synthesis and characterization of the hydrolysis behavior of **2** and its structurally characterized hydrolysis products (**3** and **4**) will be discussed in detail.

$$[Sn(ONep)_2]_\infty + nH_2O \rightarrow \text{“}Sn_w(O)_x(ONep)_y\text{”} + zHONep \quad (2)$$

Experimental Section

All compounds were handled with rigorous exclusion of air and undesired water using standard Schlenk line and glovebox techniques. All solvents were freshly distilled from the appropriate drying agent immediately prior to use.[55] The following chemicals were used as received (Aldrich), stored, and handled under an argon atmosphere: $SnCl_2$, $LiNMe_2$, and HONep. 5% ^{17}O-enriched H_2O (H_2O^*) was kindly supplied by D. L. Clark (Los Alamos National Laboratories). Analytical data were collected on crystalline material, under inert conditions, as described later. $[Sn(NMe_2)_2]_2$, **1**, was isolated from the slow addition of $SnCl_2$ to 2 equiv of $LiNMe_2$ in THF.[18,45,46]

FT-IR data were obtained on a Bruker Vector 22 spectrometer using KBr pellets under an atmosphere of flowing nitrogen. Elemental analyses were performed on a Perkin-Elmer 2400 CHN-S/O elemental analyzer. The X-ray diffraction powder data were collected using a zero background holder on a Siemens D500 $\theta-\theta$ diffractometer equipped with Cu Kα radiation, a graphite monochromator, and a scintillation detector and refined using the JADE software package. Powder samples were loaded into a plastic envelope and heat-sealed under an argon atmosphere, prior to obtaining the XRD pattern.

NMR Experimental. The solid-state MAS NMR spectra were obtained on a Bruker AMX400 using a 4 mm broadband (BB) probe. The ^{13}C CP-MAS spectra were obtained at 100.6 MHz using a 1 ms contact time, 64−128 scan averages with high-power ^1H decoupling. The ^{17}O and ^{119}Sn NMR spectra were obtained at 54.2 and 149.1 MHz, respectively, using single pulse Bloch decay with high power ^1H decoupling. Samples were spun between 10 and 15 kHz, with 4−16K scan averages for ^{17}O and 256−1024 scan averages for ^{119}Sn, and a 10 s recycle delay for the ^{17}O MAS and a 60 s delay for the ^{119}Sn MAS.

The ^1H, ^{13}C, ^{17}O, and ^{119}Sn high-resolution NMR spectra were obtained at 400.1, 100.6, 54.2, and 149.1 MHz, respectively, on a Bruker DRX400. Standard pulse sequences were used in all cases. The ^1H and ^{13}C spectra were referenced to the deuterated solvent signal. The ^{17}O NMR spectra were referenced to external H_2O ($\delta = 0.0$ ppm) while the ^{119}Sn spectra were referenced to external neat $SnMe_4$ ($\delta = 0.0$ ppm).

The $^1H-^{119}Sn$ and the $^1H-^{13}C$ 2D HMQC spectra were obtained on a Bruker Avance 600 MHz instrument using a 5 mm inverse BB probe with a *z*-gradient at a ^1H frequency of 600.1 and a ^{119}Sn frequency of 223.6 MHz. Both spectra utilized standard gradient selected HMQC pulse sequences, except as noted. Because there can exist a wide range of $^3J(^1H-^{119}Sn)$ and $^4J(^1H-^{119}Sn)$ coupling constants, especially through heteroatoms, a series of different 2D HMQC spectra optimized for coupling constants ranging from 2 through 50 Hz were performed to observe all possible couplings.[56] In addition, this range of coupling constants is known to result in phase distortions due to incomplete refocusing of the $^1H-^{119}Sn$ interaction. To overcome this difficulty, the final refocusing delay was removed from the standard HMQC sequence for the $^1H-^{119}Sn$ HMQC analysis with the data being displayed in magnitude form. This difficulty in $^1H-^{119}Sn$ correlations, along with possible sequence modifications, has been previously discussed in detail.[56]

$[Sn(ONep)_2]_\infty$ (2). To a stirring, ice-bath cooled solution of **1** (20.0 g, 96.5 mmol) in hexanes (250 mL), HONep (16.99 g, 193 mmol) was slowly added via addition tube. This is a very exothermic reaction, and the addition must be undertaken with care. After complete addition, the reaction mixture was allowed to stir to room temperature and then warmed at ~60 °C for at least 1 h to ensure completion of reaction. The resulting mixture was dried in vacuo to yield an off-white powder. The powder was slurried in hexanes and filtered through a glass frit. The precipitate was collected and used without further purification. Unoptimized yield 22.9 g (80.9%). Suitable crystals for X-ray analysis were grown by redissolution of the bulk powder in warm THF. The clear solution was allowed to cool (~5 min) yielding needlelike crystals that were acceptable for X-ray analyses. FT-IR (KBr, cm^{-1}) 2952-(s), 2899(m,sh), 2867(s), 2838(sh, m), 2712(w), 1476(m), 1460-(m,sh), 1439(w,sh), 1391(m), 1361(m), 1259(w), 1213(w), 1036(s), 1004(s), 932(w), 895(w), 583(m), 567(m), 447 (w), 423(w). ^1H NMR (400.1 MHz, 25 °C, THF-d_8) δ 3.58 (2H, s, OCH_2CMe_3), 0.94 (10H, s, OCH_2CMe_3). $^{13}C\{^1H\}$ (100.1 MHz, 45 °C, THF-d_8) δ 74.6 (OCH_2CMe_3), 67.4 (THF), 33.9 (OCH_2CMe_3), 27.1 (OCH_2CMe_3), 25.5 (THF). ^{119}Sn (149.1 MHz, 45 °C, THF-d_8) δ −361, −394, −197. Elemental Analysis for $SnO_2C_{10}H_{22}$ Calcd: 40.99, %C; 7.56, %H. Found: 40.22, %C; 7.48, %H.

Hydrolysis of 2. H_2O^* dissolved in THF was rapidly introduced by cannula transfer to a cloudy, stirring solution of **2** in THF, and after a few minutes, the reaction mixture cleared. The reaction was stirred for at least 12 h and then warmed at ~60 °C for 1 h. After this time, a major portion of the volatile component of the reaction mixture was removed in vacuo and allowed to set at room temperature. Crystals rapidly formed and were used for all analyses.

$Sn_5(O)_2(ONep)_6$ (3). Compound **2** (5.00 g, 17.1 mmol) in 200 mL of THF was used with H_2O^* (122.8 μL, 6.82 mmol) in THF (~50 mL). Crystalline yield 2.021 g (51.6%). FT-IR (KBr, cm^{-1}) 2953(s), (m), 2899(m), 2866(m), 2708(w), 1475(m), 1459(m), 1396-(m), 1361(m), 1260(w), 1212(w), 1037(s), 1007(s), 993(w), 895-(w), 669(w), 583(m), 567(m), 547(m), 446(w). ^1H NMR (400.1 MHz, toluene-d_8) δ 3.95 (1H, s, OCH_2CMe_3), 3.66 (1H, s, OCH_2-CMe_3), 3.55 (0.95H, s, OCH_2CMe_3), 0.98, 0.96, 0.94 (15.5H, multiplet of s, OCH_2CMe_3). ^{13}C (100.1 MHz, toluene-d_8) δ 77.8, 75.9, 75.3 (OCH_2CMe_3), 34.7, 34.4, 33.8, (OCH_2CMe_3), 28.7, 28.4, 27.4 (OCH_2CMe_3). ^{17}O(54.2 MHz, THF-d_8) δ 194.6 ($Sn_5(O)_2$-$(ONep)_6$), 14.7 (THF-d_8). ^{119}Sn (149.1 MHz, THF-d_8) δ −251

(54) Reuter, H.; Kremser, M. *Z. Anorg. Allg. Chem.* **1992**, *615*, 137.
(55) Perrin, D. D.; Armarego, W. L. F. *Purification of Laboratory Chemicals*, 3rd ed.; Pergamon Press: New York, 1988.
(56) Martins, J. C.; Biesemans, M.; Willen, R. *Prog. Nucl. Magn. Reson. Spectrosc.* **2000**, *36*, 271.

(4 Sn), −257 (1 Sn). Elemental Analysis for $Sn_5O_8C_{30}H_{66}$ Calcd: 31.37, %C; 5.79, %H. Found: 30.94, %C; 5.44, %H.

$Sn_6(O)_4(ONep)_4$ (4). Compound **2** (5.00 g, 17.1 mmol) in 200 mL of THF was used with H_2O^* (204.8 μL, 11.4 mmol) in THF (~50 mL). Crystalline yield 1.925 g (60.2%). FT-IR (KBR, cm^{-1}) 2954(s), 2962(m, sh), 2860(s), 2819(s), 2748(m), 2707(w), 1475-(m), 1460(w), 1450(w), 1439(w), 1397(m), 1361(m), 1261(m), 1210(w), 1099(m,sh), 1037(s), 1008(s), 931(m), 898(w), 801(m), 588(m,sh), 545(s), 466(m). ^{1}H NMR (400.1 MHz, toluene-d_8) δ 3.51 (2.1H, OCH_2CMe_3), 0.95 (9H, OCH_2CMe_3). ^{13}C (100.1 MHz, toluene-d_8) δ 76.3 (OCH_2CMe_3), 34.0 (OCH_2CMe_3), 27.2 (OCH_2-CMe_3). ^{17}O(54.2 MHz, THF-d_8) δ 197.9 ($Sn_6(O)_4(ONep)_4$), 14.8 (THF-d_8). ^{119}Sn (149.1 MHz, THF-d_8) δ −128. Elemental Analysis for $Sn_6O_8C_{20}H_{44}$ Calcd: 21.38, %C; 3.94, %H; Found: 21.20, %C; 3.76, %H.

General X-ray Crystal Structure Information.[57] Each crystal was mounted onto a thin glass fiber from a pool of Fluorolube and immediately placed under a liquid N_2 stream, on a Bruker AXS diffractometer. The radiation used was graphite monochromatized Mo Kα radiation (λ = 0.7107 Å). The lattice parameters were optimized from a least-squares calculation on carefully centered reflections. Lattice determination and data collection were carried out using SMART version 5.054 software. Data reduction was performed using SAINT Version 6.01 software, structure solutions were performed using SHELXTL 5.1 (10/29/98) software, and structure refinements were performed using XSHELL 4.1 (11/08/2000) software. The data were corrected for absorption using the SADABS (version 2.03) within the SAINT+ 6.04 (1/19/01) software.

Each structure was solved using direct methods that yielded the Sn and O atoms, along with a number of the C atoms. Subsequent Fourier synthesis yielded the remaining C atom positions. The hydrogen atoms were fixed in positions of ideal geometry and refined within the XSHELL software. These idealized hydrogen atoms had their isotropic temperature factors fixed at 1.2 or 1.5 times the equivalent isotropic U of the C atoms for which they were bonded. The final refinement of each compound included anisotropic thermal parameters on all non-hydrogen atoms. Additional information concerning the data collection and final structural solutions of **2**−**4** can be found in the Supporting Information.

$Sn_5(O)_2(ONep)_6$ (3). Upon inspection of the full data set, the crystal of **3** was found to be twinned. The Program GEMINI was employed to determine the twin relationship, which proved to be a 180° rotation axis about the (0,1,0) in reciprocal space. Lattice determination for both twin components, data reduction, and corrections for absorption were undertaken as described previously. GEMINI was again employed to separate partial overlapped reflections.

Results

Compound 2. The synthesis of "$Sn(ONep)_2$" was undertaken using an amide−alcohol exchange reaction (eq 1). $[Sn(NMe_2)_2]_2$ (**1**) was chosen as the starting amide because it was simple to synthesize,[18,45,46] quickly purified by either sublimation or crystallization, and easy to handle as a powder. The dried white powder was redissolved in hot hexanes, toluene, or THF, followed by slow cooling to form crystalline material. The THF crystals were acceptable for single-crystal X-ray analysis and proved to be polymeric compound $[Sn(ONep)_2]_\infty$ (**2**). Figure 2a shows the thermal

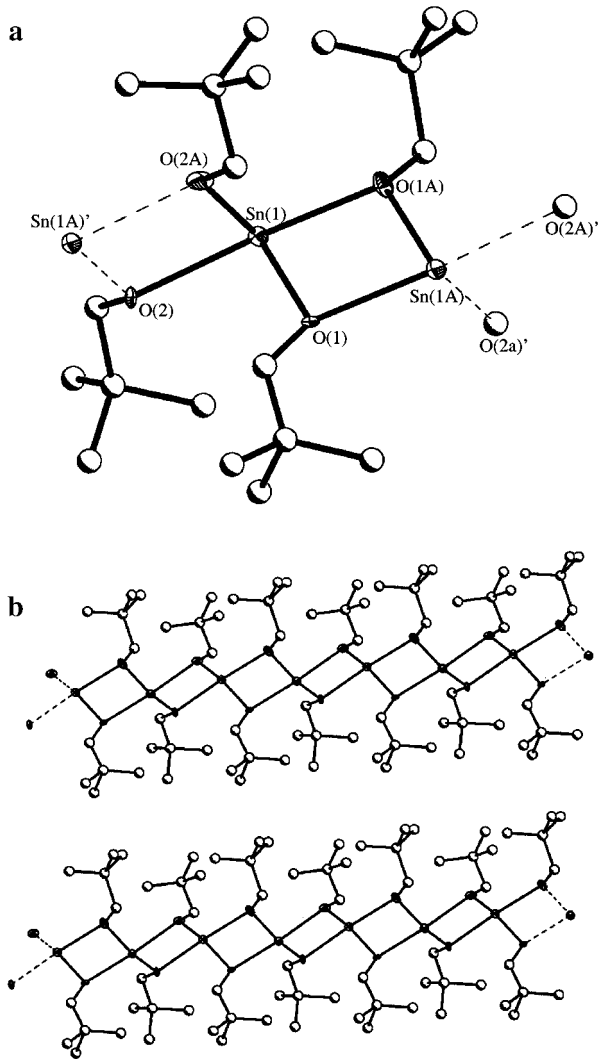

Figure 2. (a) Thermal ellipsoid plot of **2**. Thermal ellipsoids are drawn at 30%. (b) Packing diagram of polymeric chains of **2**.

Table 1. Data Collection Parameters for **2**−**4**

compound	**2**	**3**	**4**
chemical formula	$C_{20}H_{44}O_4Sn_2$	$C_{30}H_{66}O_8Sn_5$	$C_{40}H_{88}O_{16}Sn_{12}$
formula weight	585.93	1148.28	2249.38
temp (K)	168(2)	168(2)	168(2)
space group	triclinic $P\bar{1}$	triclinic $P\bar{1}$	orthorhombic $P2_12_12_1$
a (Å)	6.1757(10)	10.182(9)	23.777(3)
b (Å)	9.5349(15)	11.707(11)	23.961(3)
c (Å)	11.1180(17)	20.167(18)	11.985(2)
α (deg)	74.894(3)	87.127(12)	
β (deg)	81.359(2)	84.157(13)	
γ (deg)	85.962(3)	64.555(11)	
V (Å^3)	624.55(17)	2159(3)	6828.0(15)
Z	1	2	4
D_{calcd} (Mg/m^3)	1.558	1.766	2.188
μ(Mo Kα) (mm^{-1})	2.019	2.889	4.356
R1[a] (%)	3.13	4.60	2.28
wR2[b](%)	8.17	11.60	5.49
R1[a] (all data, %)	3.25	6.04	2.55
wR2[b] (all data, %)	8.26	12.54	5.61

[a] $R1 = \sum||F_o| - |F_c||/\sum|F_o| \times 100$. [b] $wR2 = [\sum w(F_o^2 - F_c^2)^2/\sum(w|F_o|^2)^2]^{1/2} \times 100$.

(57) The listed versions of SAINT, SMART, XSHELL, and SADABS Software from Bruker Analytical X-ray Systems Inc., 6300 Enterprise Lane, Madison, WI 53719, were used in analysis.

Table 2. Selected Metrical Data for **2**−**4**

bond (Å)	**2**		**3**		**4**	
Sn···Sn	Sn(1)···Sn(2)	3.581	Sn(1)···Sn(2)	3.443	Sn(1)···Sn(6)	3.418
	Sn(1)···Sn(2a)	3.589	Sn(1)···Sn(3)	5.066	Sn(1)···Sn(2)	3.564
			Sn(1)···Sn(4)	3.714	Sn(1)···Sn(5)	3.569
			Sn(1)···Sn(5)	3.569	Sn(1)···Sn(3)	3.625
			Sn(2)···Sn(3)	3.646	Sn(1)···Sn(4)	5.014
			Sn(2)···Sn(4)	5.015	Sn(2)···Sn(3)	3.437
			Sn(2)···Sn(5)	3.559	Sn(2)···Sn(4)	3.533
			Sn(3)···Sn(4)	3.446	Sn(2)···Sn(6)	3.635
			Sn(3)···Sn(5)	3.593	Sn(2)···Sn(5)	5.023
			Sn(4)···Sn(5)	3.509	Sn(3)···Sn(5)	3.431
					Sn(3)···Sn(4)	3.624
					Sn(3)···Sn(6)	4.962
					Sn(4)···Sn(5)	3.570
					Sn(4)···Sn(6)	3.446
					Sn(5)···Sn(6)	3.623
Sn−(μ-ONep)	Sn(1)−O(1)	2.114(3)	Sn(1)−O(3)	2.200(9)	Sn(1)−O(5)	2.206(4)
	Sn(1)−O(2)	2.122(3)	Sn(1)−O(7)	2.127(9)	Sn(2)−O(6)	2.192(5)
	Sn(1)−O(2)#1	2.374(3)	Sn(2)−O(3)	2.317(8)	Sn(3)−O(7)	2.195(5)
	Sn(1)−O(1)#2	2.403(3)	Sn(2)−O(4)	2.143(9)	Sn(4)−O(7)	2.373(5)
			Sn(3)−O(4)	2.189(9)	Sn(4)−O(8)	2.346(4)
			Sn(3)−O(6)	2.252(9)	Sn(5)−O(5)	2.360(4)
			Sn(4)−O(6)	2.205(9)	Sn(5)−O(6)	2.329(5)
			Sn(4)−O(7)	2.164(8)	Sn(6)−O(8)	2.199(5)
Sn−(μ_3-ONep)			Sn(2)−O(5)	2.288(9)		
			Sn(3)−O(5)	2.359(10)		
			Sn(4)−O(8)	2.447(9)		
			Sn(5)−O(8)	2.211(8)		
			Sn(5)−O(5)	2.58(2)		
			Sn(1)−O(8)	2.63(2)		
Sn−(μ_3-O)			Sn(1)−O(1)	2.035(8)	Sn(1)−O(1)	2.067(4)
			Sn(2)−O(1)	2.092(8)	Sn(1)−O(2)	2.076(4)
			Sn(3)−O(2)	2.067(9)	Sn(2)−O(3)	2.071(4)
			Sn(4)−O(2)	2.063(9)	Sn(2)−O(4)	2.081(4)
			Sn(5)−O(2)	2.029(9)	Sn(3)−O(1)	2.082(4)
			Sn(5)−O(1)	2.060(8)	Sn(3)−O(4)	2.075(4)
					Sn(4)−O(1)	2.099(4)
					Sn(4)−O(3)	2.102(5)
					Sn(5)−O(4)	2.086(5)
					Sn(5)−O(2)	2.103(4)
					Sn(6)−O(2)	2.067(4)
					Sn(6)−O(3)	2.086(4)

angle (deg)	**2**		**3**		**4**	
Sn−(μ-ONep)−Sn	Sn(1)−O(2)−Sn(1)#1	105.43(12)	Sn(1)−O(3)−Sn(2)	99.3(4)	Sn(1)−O(5)−Sn(5)	96.90(16)
	Sn(1)−O(1)−Sn(1)#2	105.06(12)	Sn(2)−O(4)−Sn(3)	112.7(4)	Sn(2)−O(6)−Sn(5)	98.9(2)
			Sn(2)−O(5)−Sn(3)	101.8(4)	Sn(3)−O(7)−Sn(4)	97.37(17)
			Sn(4)−O(6)−Sn(3)	101.6(4)	Sn(6)−O(8)−Sn(4)	97.55(17)
			Sn(1)−O(7)−Sn(4)	121.4(5)		
			Sn(5)−O(8)−Sn(4)	95.8(3)		
Sn−(μ_3-O)−Sn			Sn(1)−O(1)−Sn(2)	113.1(4)	Sn(1)−O(1)−Sn(3)	118.5(2)
			Sn(1)−O(1)−Sn(5)	120.8(4)	Sn(1)−O(1)−Sn(4)	120.62(19)
			Sn(2)−O(1)−Sn(5)	120.4(3)	Sn(3)−O(1)−Sn(4)	110.40(19)
			Sn(3)−O(2)−Sn(4)	113.6(5)	Sn(6)−O(2)−Sn(1)	119.05(19)
			Sn(3)−O(2)−Sn(5)	123.0(4)	Sn(6)−O(2)−Sn(5)	119.05(19)
			Sn(4)−O(2)−Sn(5)	115.4(4)	Sn(1)−O(2)−Sn(5)	120.5(2)
					Sn(1)−O(2)−Sn(5)	109.76(19)
					Sn(2)−O(3)−Sn(6)	118.7(2)
					Sn(2)−O(3)−Sn(4)	120.8(2)
					Sn(6)−O(3)−Sn(4)	109.5(2)
					Sn(3)−O(4)−Sn(2)	116.8(2)
					Sn(3)−O(4)−Sn(5)	121.3(2)
					Sn(2)−O(4)−Sn(5)	111.1(2)
(μ-ONep)−Sn−(μ-ONep)	O(1)−Sn(1)−O(2)	92.67(13)	O(4)−Sn(2)−O(5)	72.5(4)	O(7)−Sn(4)−O(4)	83.10(18)
	O(1)−Sn(1)−O(2)#1	93.55(11)	O(4)−Sn(2)−O(3)	86.3(3)	O(5)−Sn(5)-O(6)	141.46(16)
	O(2)−Sn(1)−O(2)#1	74.57(12)	O(4)−Sn(3)−O(6)	86.8(3)		
	O(1)−Sn(1)−O(1)#2	74.94(12)	O(4)−Sn(3)−O(5)	70.3(3)		
	O(2)−Sn(1)−O(1)#2	92.82(11)	O(5)−Sn(2)−O(3)	140.2(3)		
	O(2)#1−Sn(1)−O(1)#2	162.71(12)	O(6)−Sn(3)−O(5)	137.3(3)		
			O(6)−Sn(4)−O(8)	138.2(3)		
			O(7)−Sn(1)−O(3)	90.2(3)		
			O(7)−Sn(4)−O(6)	89.7(3)		
			O(7)−Sn(4)−O(8)	74.3(3)		

Table 2 (Continued)

angle (deg)	2	3	4
(μ_3-O)−Sn−(μ_3-O)		O(1)−Sn(5)−O(2) 89.9(3)	
(μ_3-O)−Sn−(μ-ONep)		O(1)−Sn(1)−O(7) 94.1(3) O(1)−Sn(1)−O(3) 75.5(3) O(1)−Sn(2)−O(3) 71.9(3) O(1)−Sn(2)−O(4) 96.7(3) O(1)−Sn(2)−O(5) 77.5(3) O(1)−Sn(5)−O(8) 79.0(3) O(2)−Sn(4)−O(7) 97.1(3) O(2)−Sn(3)−O(5) 76.3(3) O(2)−Sn(3)−O(4) 97.6(3) O(2)−Sn(3)−O(6) 71.6(4) O(2)−Sn(4)−O(6) 72.6(4) O(2)−Sn(5)−O(8) 77.3(3) O(2)−Sn(4)−O(8) 71.5(3)	

Table 3. MAS and CPMAS Data for **1**−**4**

cmpd	^{13}C	^{17}O[a] (QCC MHz, η)	^{119}Sn
1	46.8, 44.7 (N*Me*$_2$)	*b*	+210
2	75.6, 74.4 (OCH_2CMe$_3$) 35.2, 34.1,(OCH$_2$*C*Me$_3$) 29.3, 29.7 (OCH$_2$C*Me*$_3$)	*b*	−214
3	78.1, 75.2 (OCH_2CMe$_3$) 34.8, 34.3, 33.7 (OCH$_2$*C*Me$_3$) 30.1, 29.4, 28.4 (OCH$_2$C*Me*$_3$)	+195 (3.54, ∼0.0)	−159.0 (1 Sn) −175.5 (2 Sn) −194.9 (2 Sn)
4	76.0 (O*C*H$_2$CMe$_3$) 34.6 (OCH$_2$*C*Me$_3$) 28.1 (OCH$_2$C*Me*$_3$)	+199 (3.89, ∼0.2)	−51.9 −61.4

[a] ^{17}O chemical shift (ppm) along with the quadrupolar coupling constant (QCC) and quadrupolar asymmetry parameter (η) were obtained from simulations of the second-order quadrupolar coupled MAS spectra. [b] No ^{17}O CP-MAS data were collected for these samples because they were not enriched.

ellipsoid plot of **2** with the packing diagram of the polymeric chains shown in Figure 2b. Data collection parameters for **2** are listed in Table 1, and selected metrical data are listed in Table 2. For **2**, each metal center is coordinated by four ONep ligands, forming a bent chain (Figure 2b). If the free electron pair of each Sn^{2+} metal center is considered in the overall geometry (i.e., stereochemically active), a trigonal bipyramidal (TBP) arrangement is observed with the free electron pair located in one of the equatorial sites. The metrical data for **2** are consistent with literature reports: Sn−O, av 2.25 Å; Sn−(μ-OR)−Sn, av 105.2°; (μ-OR)−Sn−(μ-OR), range 74.57°−162.71°.[22−24,26,27]

To further characterize the bulk properties of **2**, additional analytical data were obtained. Elemental analyses of the bulk powder were consistent with the solid-state structure. The FT-IR spectrum of **2** revealed standard ONep stretches with no OH stretches observed around 3000 cm^{-1}. In the M−O region,[18] the broad stretch observed at 567 cm^{-1} and a small shoulder at 583 cm^{-1} were assigned to Sn−(μ-ONep), in agreement with literature reports.[18] The solid-state MAS (^{13}C, ^{119}Sn) NMR data of **2** are tabulated in Table 3 and reveal the presence of two types of ONep ligands and a single Sn site. The inequivalent ONep resonances in the ^{13}C spectrum may be due to the equatorial and axial ligands of the TBP Sn metal center or molecular packing derived inequivalencies. The bulk powder was sealed in a heat-sealed plastic envelope, and the XRD powder pattern was collected. The majority of the peaks of the resultant spectrum were consistent with the idealized XRD pattern generated from the single-crystal data.[57] Any variations noted are due to the fact that the actual powder was not completely randomized.

Because metal alkoxides are often dynamic in solution, it was also important to understand the solution behavior of **2**. Both the ^{1}H and ^{13}C solution NMR spectra in THF-d_8 revealed only one set of ONep resonances. Attempts to obtain a solution ^{119}Sn spectrum of **2** were not successful at room temperature; however, a minor very broad resonance was noted around δ −197 ppm. The NMR tube of **2** in THF-d_8 was opaque, indicative of the low solubility of **2** in THF, which would explain the lack of a ^{119}Sn signal. At higher temperatures (45 °C), the solution was clear, and three ^{119}Sn resonances were observed. ^{119}Sn NMR chemical shifts have been shown to be highly dependent upon the coordination environment of the cation.[58] Because of the conflicting ^{119}Sn assignments of the 2-coordinated Sn(OCBu$^t_3$)$_2$,[58] (δ = −165 ppm), the 3-coordinated [Sn(μ-OSiMe$_3$)(OSiMe$_3$)]$_2$ complex in toluene-d_8 (δ −220 ppm at room temperature[59]), and other 3- and 4-coordinated Sn−OR species,[58] exact assignment of these chemical shifts is difficult. However, the multiple number of ^{119}Sn signals observed indicates that the polymeric chain of **2** is disrupted in solution (especially at high temperature), forming shorter oligomeric chains. Attempts to obtain isopiestic molecular weight determinations were not successful because of preferential crystallization of **2** at meaningful concentrations.

Hydrolysis Products. The hydrolysis behavior of **2** in THF-d_8 was followed by ^{119}Sn NMR through the stoichiometric addition of H_2O. Two compounds were found to dominate these spectra and were subsequently synthesized on a larger scale based on the optimal stoichiometry noted during the titration. There are several methods for addition of water, but in order to minimize localized hydrolysis, it was decided to disperse the water in a solvent prior to rapid addition to **2**. The alternative methods investigated which included slow evaporation or direct addition of H_2O were also found to yield identical products.

To a stirring slurry of **2** in THF, H_2O* (O-17 labeled) in THF was added via cannula. In less than 5 min, the solution cleared. After 12 h, the clear, yellow-tinged reaction was warmed slightly, followed by in vacuo removal of the

(58) Teff, D. J.; Minear, C. D.; Baxter, D. V.; Caulton, K. G. *Inorg. Chem.* **1998**, *37*, 2547.
(59) Sita, L. R.; Babcock, J. R.; Xi, R. *J. Am. Chem. Soc.* **1996**, *118*, 10912.

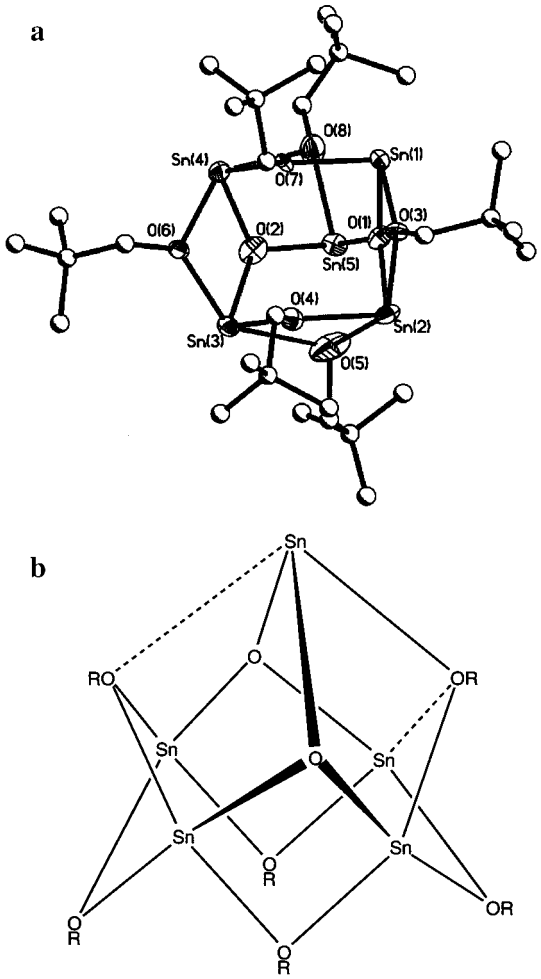

Figure 3. (a) Thermal ellipsoid plot of **3**. Thermal ellipsoids are drawn at 30%. (b) Schematic representation of **3** (note: the dashed lines are too long in the solid state to be considered bonds).

majority of the volatile components. X-ray quality crystals formed after a short time (<1 h). When the stoichiometry of the added water (*n* in eq 2) was kept close to $n = {}^{2}/_{5}$, $Sn_5(O)_2(ONep)_6$ (**3**) was isolated, but when increased to $n = {}^{2}/_{3}$, $Sn_6(O)_4(ONep)_4$ (**4**) was isolated. Figures 3a and 4 show the thermal ellipsoid plots of **3** and **4**, respectively. Once formed, the hydrolysis products (**3** and **4**) were significantly more soluble than the parent alkoxide, **2**.

Additional analytical data were collected on the bulk powders to determine if they were consistent with the single-crystal structures. Elemental analyses of the powders of **3** and **4** were all within agreement for the solid-state structures. The absence of stretches at 3000 cm^{-1} in the FT-IR spectra of **3** and **4** is indicative of a lack of coordinated HONep and/or H_2O in the final products. The IR spectra of **2**−**4** are very similar because the ONep stretches and bend dominate the spectra wherein the major differences occur in the metal oxide region.[18] In the M−O region,[18] for **3**, there are three strong stretches (583, 567, 547 cm^{-1}) but only two (588, 545 cm^{-1}) for **4**. Elimination of the Sn−(μ-ONep) stretches as assigned for **2**[18] (vide supra) left the stretch at 585 cm^{-1} which was tentatively assigned as the Sn−(μ_3-O) stretch. The majority of the peaks observed for the bulk powder XRD

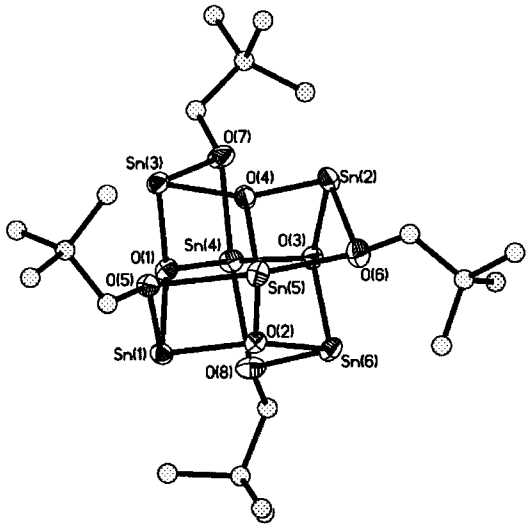

Figure 4. Thermal ellipsoid plot of **4**. Thermal ellipsoids are drawn at 30%.

powder pattern were consistent with the idealized pattern calculated from the single-crystal data.[57]

Previous reports on hydrolyzed $Sn(OR)_2$ indicate that these compounds undergo a two step hydrolysis mechanism, but these intermediates were not structurally characterized.[51,52] As mentioned previously, the majority of structurally characterized hydrolyzed products of $Sn(OR)_2$ compounds belong to the $Sn_6(\mu_3\text{-}O)_4(\mu_3\text{-}OR)_4$ (OR = OH,[48] OMe,[49] $OCHMe_2$[50]) family. Furthermore, the self-etherification of the reported $[Sn(OSiMe_3)_2]_2$ led to an identical core structure as noted.[53] These $Sn_6(\mu_3\text{-}O)_4(\mu_3\text{-}OR)_4$ compounds adopt a ball-like structure consisting of edge-shared $[Sn{-}OR]_2$ squares (Figure 1), wherein each Sn cation adopts a 4-coordinated pyramidal (PYD) geometry linked by triply bridging ligands. The structures of **3** and **4** are novel in comparison to the previously identified partially condensed complexes and structurally define the hydrolysis behavior of **2**. Data collection parameters are listed in Table 1, and metrical data are listed in Table 2.

Compound 3. The structure of **3** consists of a square base pyramidal arrangement of Sn atoms and is shown in Figure 3a. Each of the basal metals is bridged by two μ-ONep ligands. Two opposing faces of the apical and basal Sn atoms are bridged by μ_3-O ligands. On the opposite faces, there are two μ-ONep ligands, one of which binds between a basal and the apical Sn atom and the other bridges between only the basal Sn metal centers which results in an asymmetric molecule. For this discussion, we are assigning Sn−O distances of <2.5 Å as "true" Sn−O bonds. Therefore, two of the facial μ-ONep ligands that have significantly longer Sn−OR distances [Sn(5)−O(5) 2.58(2) Å and Sn(1)−O(8) 2.63(2) Å] were not considered bonding (Figure 3b). This leads to three of the Sn cations being 4-coordinated and two being 3-coordinated. Because of the presence of the free electron pairs and the weak ligand metal interactions, the various Sn metal centers adopt either a distorted TBP or tetrahedral geometry. The Sn−OR and Sn−(μ_3-O) distances of **3** are shorter, av 2.19 and 2.06 Å, respectively, than those

noted for the Sn−(μ-OR) distances of **2**, and the Sn−(μ_3-OR) distance (av 2.33 Å) was longer.

On the basis of the described structure, compound **3** has no equivalent ONep ligands or Sn cations. The ^{13}C MAS spectrum (Table 3) displayed three types of ONep ligands, the ^{119}Sn MAS spectrum had three resonances in a 1:2:2 ratio, and the ^{17}O MAS NMR spectrum revealed only one oxygen resonance. Because the ^{17}O enrichment will only be incorporated into the hydrolyzed site via the addition of H_2O*, only the oxo species will be labeled and are expected to be equivalent. Because of the second order quadrupolar broadening of these resonances, small differences in the oxo-oxygen types were not resolvable in these experiments. The three different ONep ligand resonances may be a result of overlapping ONep resonances in very similar environments. For instance, if the interactions of the O(5) and O(8) ONep ligands are strong enough, they may approximate μ_3-ONep ligands (a schematic representation is shown in Figure 3b), and then three types of ONep ligand environments are expected: two μ_3-ONep, two μ-ONep ligands bridged on the opposite side by μ_3-ONep, and two μ-ONep ligands bridged on the opposite side by the μ_3-O ligands. The ^{119}Sn nucleus is more sensitive to environmental changes than the ^{13}C nuclei, and thus, the asymmetry noted for the solid-state structure would be more easily observed with one apical and two types of disparate basal Sn cations. The bulk powder XRD pattern was consistent with the idealized XRD powder pattern generated from the single-crystal data.[57]

In an effort to determine the solution behavior of **3**, ^{1}H, ^{13}C, ^{17}O, and ^{119}Sn NMR spectra were obtained. One set of ONep resonances was observed for the ^{1}H and ^{13}C NMR spectrum of **3**. The ^{17}O NMR spectrum revealed two resonances at δ 194.6 and 14.7 ppm that were assigned as a resonance from the enriched oxo ligands and a resonance from the neat natural abundance THF-d_8 solvent, respectively.[60] The solution ^{119}Sn NMR spectrum had two resonances in a 4:1 ratio that were observed at δ −251 and −257 ppm, respectively. If the asymmetric solid-state structure of **3** is retained in solution, there should be five types of ^{119}Sn resonances; however, with minimal ligand redistribution, the $Sn_5(\mu_3\text{-}O)_2(\mu_3\text{-}ONep)_2(\mu\text{-}ONep)_4$ species could easily form (Figure 3b). The one apical and four equivalent basal Sn cations would each be 4-coordinated, explaining the similar chemical shifts and ratio of observed resonance. However, the ^{119}Sn chemical shifts observed for **3** are more in line with 3-coordinated Sn species[58] (4-coordinated Sn(IV) alkoxide complex [Sn(O^{t}Bu)$_4$ (δ −352)[58] and Sn(O^{t}Am)$_4$ (δ −370)[30]] and the two coordinated Sn(OCBu$^t_3$)$_2$ (δ −165 ppm)[58]). This inconsistency may be due to several other variables including the mixed ligand set of **3**, the polar solvent used for dissolution, and concentration effects, all of which will influence the sensitive Sn chemical shift.[58] Surprisingly, the $^{117-119}$Sn ^2J-coupling that would indicate Sn−O−Sn linkages (range from 223[30,61] to 420−440[22,58,62]

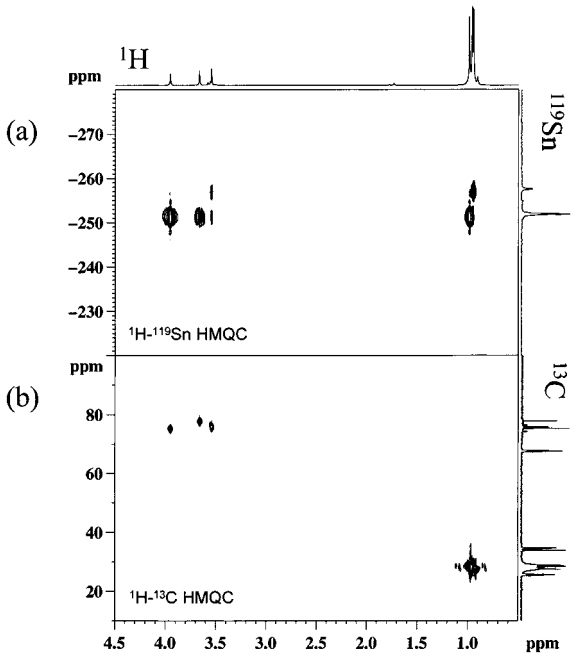

Figure 5. Gradient selected 2D (a) ^{1}H−^{119}Sn and (b) ^{1}H−^{13}C HMQC of **3**. The two spectra are joined together because they share a common ^{1}H dimension.

Table 4. Summary of Assignments from High Resolution 2D Solution NMR Data for **3** in THF-d_8

nucleus	assignment			
^{1}H	CH_2	3.95	3.66	3.55
	CH_3	0.98	0.96	0.94
^{119}Sn		−251.9	−251.9	−257, −251.9
^{13}C	CH_2	75.3	77.8	75.9
	C	33.8	34.7	34.4
	CH_3	28.7	28.4	27.4

to 610 Hz[58]) was *not* observed for **3**. This phenomena was attributed to rapid ligand exchange, which caused fluctional distortions in the coordination of the Sn^{2+} metal centers. This phenomena was also previously reported for the similar $Sn_6O_4(OSiMe_3)_4$ compound.[53]

To further assign the various resonances, ^{1}H−^{119}Sn and ^{1}H−^{13}C 2D NMR spectra were collected and shown in Figure 5a and b, respectively. By utilizing both ^{1}H−^{119}Sn and ^{1}H−^{13}C HMQC, along with ^{1}H−^{13}C HMBC experiments, correlations, through the ^{1}H, can be used to assign all of the nonequivalent ^{13}C and ^{1}H resonances. Table 4 lists the various resonances that were observed. Correlations between the ^{1}H resonance at δ = 3.55 ppm of the CH_2 group to both of the Sn resonances at −257 and −251.9 via ^3J(^{1}H−^{119}Sn) and ^4J(^{1}H−^{119}Sn) coupling show that this ^{1}H resonance represents the μ_3-ONep ligands. The single Sn correlation of the δ 3.95 and 3.66 ppm resonances suggests that these resonances are due to the terminal ONep ligands. A distinction between the two nonequivalent ONep resonances was not realized. Combined, the solution state NMR data indicate that, in solution, while there is some ligand redistribution to form a more symmetrical molecule (Figure 3b), the central core of the solid structure of **3** is maintained in solution.

(60) *^{17}O NMR Spectroscopy in Organic Chemistry*; Boykin, D. W., Ed.; CRC Press: Boston, 1991.
(61) Lockhart, T. P.; Puff, H.; Schuh, W.; Reuter, H.; Mitchell, T. N. *J. Organomet. Chem.* **1989**, *366*, 61.
(62) Boegeat, D.; Jousseaume, B.; Toupance, T.; Campet, G.; Fournes, L. *Inorg. Chem.* **2000**, *39*, 3924.

Compound 4. For **4**, the Sn atoms adopt an octahedral arrangement with an S_4 axis of symmetry. Each cis equatorial Sn atom bridges one of four μ_3-O ligands to an axial Sn cation in an oscillatory pattern. The equatorial Sn(5) cation bridges one μ-ONep ligand to each axial Sn atom. The Sn(4) cation, trans to Sn(5), bridges one μ-ONep to the equatorial Sn(5) and Sn(6). The axial Sn atoms are in a formally 4-coordinated pyramidal geometry but with the inclusion of the lone pair form a 5-coordinated square base pyramidal geometry. Considering the lone pair in the geometrical arrangement, two of the equatorial Sn atoms are 5-coordinated (Sn(4) and Sn(5)) forming a square base pyramidal geometry, and two are 4-coordinated (Sn(3) and Sn(6)) yielding tetrahedral geometries. In contrast to the other reported structures of the $Sn_6(\mu_3\text{-}O)_4(\mu_3\text{-}OR)_4$ family (Figure 1), **4** does not form any μ_3-OR bonds. The distances are too long to formally be classified as bonding; however, there must be some interaction based on the metrical data. This phenomenon must be due to the steric bulk of the ONep, which has repeatedly yielded compounds of reduced nuclearity in comparison to the other small chain alkoxides.[36−44] The Sn−(μ-ONep) distances (2.192−2.373 Å) and the Sn−(μ_3-O) distances (2.067−2.103 Å) are consistent with those observed for **2**, **3**, and literature values.[22−24,26,27]

If the bulk powder is consistent with the crystal structure of **4**, there should be two types of μ-ONep, two types of μ_3-O, and four types of Sn cations. The ^{13}C and ^{17}O MAS NMR spectra reveal only one set of resonances (see Table 3) and two resonances for the ^{119}Sn MAS NMR spectrum (δ −51.9 and −61.4 ppm; *note*: the exact ratio of these two resonances could not be obtained because of the extremely broad, chemical shift anisotropy, spinning sideband manifold observed). These resonances are significantly downfield from those noted for **3** which must be a result of the increased amount of oxo ligand and change in coordination. The subtle differences in the basal bridging and facial bridging μ-ONep ligands may not be detectable by ^{13}C and ^{17}O MAS NMR. ^{119}Sn resonances are well-known to be sensitive to their coordination environment, and the two resonances most likely represent the 3- and 4-coordinated Sn cations present in **4** but are significantly varied from that of **3**. Therefore, these data coupled with the XRD powder information, confirm that the bulk sample is consistent with the crystal structure.

The solution behavior of the ^{17}O-enriched **4** was investigated using ^{1}H, ^{13}C, ^{17}O, and ^{119}Sn NMR spectroscopy. The ^{1}H and ^{13}C solution state NMR spectra of **4** had one set of resonances for the ONep ligands. The ^{17}O NMR data of the H_2O*-enriched **4** revealed two types of oxygen environments at 197.9 (μ_3-O) and 14.8 ppm (THF), as noted for **3**, and the ^{119}Sn NMR possessed only a single resonance at −128 ppm. In solution, it is reasonable to believe that the weak interactions are averaged over the molecule (i.e., dynamic ligand scrambling) yielding a very symmetric molecule as shown in Figure 1. This is also consistent with the observed ^{119}Sn singlet. The ^{119}Sn resonance at δ −128 is upfield when compared to the signal of the siloxane derivative (δ −137.8); however, this may be more of a reflection of the ligand than the coordination geometry. On the basis of the data, it appears that the more general, symmetric molecule (Figure 1) exists in solution. Again, no $^{117-119}$Sn^2 *J*-coupling was observed in the spectrum which was possibly due to rapid ligand exchange as previously reported for $Sn_6O_4(OSiMe_3)_4$[53] and discussed here for **3**.

Solid-state NMR experiments were undertaken on a quenched reaction from eq 2 in an attempt to identify any intermediate species that might be formed during the synthesis of **3** or **4**. Initially, the reaction mixture (eq 2) was generated using $n = {}^2/_5$ H_2O. The reaction was stirred for ~3 s and was long enough to observe the initial opaqueness begin to disappear. The reaction was immediately placed in a liquid nitrogen bath and put under vacuum to remove the volatile components. The reaction was dried in vacuo for 12 h, and the resulting powder was packed into a solid-state rotor. The MAS ^{119}Sn NMR spectrum showed several resonances that correspond to the resonances for **3** and **4**. The ^{17}O-enriched MAS ^{17}O NMR spectrum of the same powder revealed two resonances consistent with **3** and **4**, along with another small, unidentified resonance at δ 379.3 ppm. Hydrolysis of metal alkoxides is often thought to proceed through a hydroxy intermediate,[18,19,21,63] but unfortunately, these quenched ^{17}O and ^{119}Sn MAS NMR experiments did not provide conclusive evidence for a OH-containing Sn(II) intermediate.

Summary and Conclusion

We have synthesized a novel polymeric Sn(II) precursor $[Sn(ONep)_2]_\infty$ (**2**) which upon hydrolysis initially forms $Sn_5(O)_2(ONep)_6$ (**3**) and then $Sn_6(O)_4(ONep)_4$ (**4**). The steric bulk of the ONep ligand leads to unique structural types. For **2**, the polymer can be disrupted by heating, yielding soluble oligomers. The hydrolysis products (**3** and **4**) are more soluble than **2**, with **3** being volatile enough for chemical vapor deposition applications. Multinuclear and multidimensional NMR investigations indicate that **2**−**4** maintain their central core in solution; however, the solid-state asymmetries of **3** and **4** are destroyed in solution yielding highly symmetric species. An uncharacterized hydroxyl intermediate has been proposed as the first step in the synthesis of **3** and **4**, but identification of this species was not fully realized. The stepwise structurally characterized hydrolysis products of **2** give insight into the construction of the final ceramic cassiterite from the parent alkoxide.

Acknowledgment. For support of this research, the authors would like to thank the Office of Basic Energy Sciences of the Department of Energy and the United States Department of Energy under Contract DE-AC04-94AL85000. Sandia is a multiprogram laboratory operated by Sandia Corporation, a Lockheed Martin Company, for the United States Department of Energy.

Supporting Information Available: Tables of crystallographic data and CIF file containing crystallographic information. This material is available free of charge via the Internet at http://pubs.acs.org.

IC011247F

(63) Bradley, D. C. *Chem. Rev.* **1989**, *89*, 1317.